NASA TN D-1822

30p.

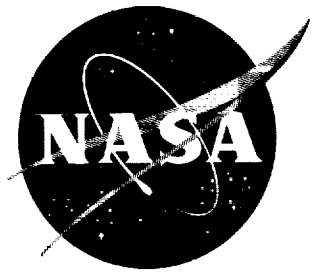

TECHNICAL NOTE

D-1822

LOW-SUBSONIC MEASUREMENTS OF STATIC AND DYNAMIC STABILITY DERIVATIVES OF SIX FLAT-PLATE WINGS HAVING LEADING-EDGE SWEEP ANGLES OF 70° TO 84°

By Robert E. Shanks

Langley Research Center
Langley Station, Hampton, Va.

NATIONAL AERONAUTICS AND SPACE ADMINISTRATION
WASHINGTON

July 1963

NATIONAL AERONAUTICS AND SPACE ADMINISTRATION

TECHNICAL NOTE D-1822

LOW-SUBSONIC MEASUREMENTS OF STATIC AND DYNAMIC STABILITY DERIVATIVES OF SIX FLAT-PLATE WINGS HAVING LEADING-EDGE SWEEP ANGLES OF 70° TO 84°

By Robert E. Shanks

SUMMARY

An investigation has been made to determine the low-speed static stability characteristics and the rolling and yawing dynamic stability derivatives of a series of thin flat-plate delta wings having leading-edge sweep angles of 70° to 84°. The investigation showed that the static longitudinal stability, the directional stability, and the effective dihedral increased with increasing sweep. The static lateral derivatives were linear at low angles of attack but became increasingly nonlinear with increase in angle of attack and increase in sweep. The values of the rolling and yawing oscillation derivatives were generally small and relatively unaffected by sweep at the lower lift coefficients but very large values of the derivative were obtained at the higher lift coefficients for the higher sweep angles. The theoretical prediction of the longitudinal stability, effective dihedral, and lateral oscillation derivatives (except C_{l_r}) at low lift coefficients is in fairly good agreement with the measured values.

INTRODUCTION

The present investigation was made in order to determine the stability characteristics of delta wings having the sweep angles being considered for some high-speed and reentry configurations. References 1 and 2 present data for delta wings having a wide range of leading-edge sweep angles up to 82.9° and 86.5°, respectively. The data of reference 1 show large changes in some of the derivatives between the sweep angles of 76° and 82.9°. Because neither of the investigations of references 1 and 2 considered wings with intermediate sweep angles, the present investigation was made in order to determine in more detail the stability characteristics of delta wings in this sweep range. The wings had sweep angles of 70°, 76°, 78°, 80°, 82°, and 84° and a thin flat-plate cross section. Static tests were made for all the wings through an angle-of-attack range of -2.5° to 40° and rolling and yawing oscillation tests were made for all the wings except the 70° wing through an angle-of-attack range of 0° to 40°.

SYMBOLS

The longitudinal data are referred to the wind axes and all lateral stability data are referred to the body system of axes (see fig. 1) originating at the moment reference position of 40.0 percent of the mean aerodynamic chord of each wing. All measurements are reduced to standard coefficient form and are based on the area and span or mean aerodynamic chord of the respective wings. The coefficients are presented in terms of the following symbols:

A	aspect ratio, b^2/S
a	length from center of gravity to trailing edge, in.
b	wing span, ft
$\bar{c}$	mean aerodynamic chord, ft
c_r	root chord, in.
D	drag, lb
F_Y	side force, lb
k	reduced-frequency parameter, $\omega b/2V$
L	lift, lb
L/D	lift-drag ratio
M_X	rolling moment, ft-lb
M_Y	pitching moment, ft-lb
M_Z	yawing moment, ft-lb
p	rolling velocity, radians/sec
$\dot{p}$	rolling acceleration, dp/dt, radians/sec^2
q	free-stream dynamic pressure, lb/sq ft
R	radius, in.
r	yawing velocity, radians/sec
$\dot{r}$	yawing acceleration, dr/dt, radians/sec^2
S	wing area, sq ft
t	time, sec

v lateral velocity, ft/sec

V free-stream velocity, ft/sec

X_{cg} distance from two-thirds root-chord station to center of gravity

X,Y,Z body reference axes unless otherwise noted

α angle of attack, deg

β angle of sideslip, $\sin^{-1}\frac{v}{V}$, deg or radians

$\dot{\beta} = \frac{d\beta}{dt}$

Λ angle of sweep, deg

φ angle of roll, radians

ψ angle of yaw, radians

$\omega = 2\pi f$ radians/sec

C_D drag coefficient, D/qS

C_l rolling-moment coefficient, M_X/qSb

$C_{l_\beta} = \frac{\partial C_l}{\partial \beta}$ per degree or per radian

C_L lift coefficient, L/qS

C_{L_α} lift-curve slope per degree

C_m pitching-moment coefficient, $M_Y/qS\bar{c}$

C_n yawing-moment coefficient, M_Z/qSb

$C_{n_\beta} = \frac{\partial C_n}{\partial \beta}$ per degree or per radian

C_Y side-force coefficient, F_Y/qS

$C_{Y_\beta} = \frac{\partial C_Y}{\partial \beta}$ per degree or per radian

$C_{l_r} = \frac{\partial C_l}{\partial \frac{rb}{2V}}$ $\quad C_{n_r} = \frac{\partial C_n}{\partial \frac{rb}{2V}}$ $\quad C_{Y_r} = \frac{\partial C_Y}{\partial \frac{rb}{2V}}$

$$C_{l_p} = \frac{\partial C_l}{\partial \frac{pb}{2V}} \qquad C_{n_p} = \frac{\partial C_n}{\partial \frac{pb}{2V}} \qquad C_{Y_p} = \frac{\partial C_Y}{\partial \frac{pb}{2V}}$$

$$C_{l_{\dot{\beta}}} = \frac{\partial C_l}{\partial \frac{\dot{\beta}b}{2V}} \qquad C_{n_{\dot{\beta}}} = \frac{\partial C_n}{\partial \frac{\dot{\beta}b}{2V}} \qquad C_{Y_{\dot{\beta}}} = \frac{\partial C_Y}{\partial \frac{\dot{\beta}b}{2V}}$$

$$C_{l_{\dot{r}}} = \frac{\partial C_l}{\partial \frac{\dot{r}b^2}{4V^2}} \qquad C_{n_{\dot{r}}} = \frac{\partial C_n}{\partial \frac{\dot{r}b^2}{4V^2}} \qquad C_{Y_{\dot{r}}} = \frac{\partial C_Y}{\partial \frac{\dot{r}b^2}{4V^2}}$$

$$C_{l_{\dot{p}}} = \frac{\partial C_l}{\partial \frac{\dot{p}b^2}{4V^2}} \qquad C_{n_{\dot{p}}} = \frac{\partial C_n}{\partial \frac{\dot{p}b^2}{4V^2}} \qquad C_{Y_{\dot{p}}} = \frac{\partial C_Y}{\partial \frac{\dot{p}b^2}{4V^2}}$$

The term "in-phase derivative" used herein refers to any one of the oscillatory derivatives that are based on the components of forces and moments in phase with the angle of roll or yaw produced in the oscillatory tests. The term "out-of-phase derivative" refers to any one of the stability derivatives which is based on the components of the forces and moments 90° out of phase with the angle of roll or yaw. The oscillatory derivatives of the present investigation were measured in the following combinations:

$$\left.\begin{array}{l} C_{l_p} + C_{l_{\dot{\beta}}} \sin\alpha \\ C_{n_p} + C_{n_{\dot{\beta}}} \sin\alpha \\ C_{Y_p} + C_{Y_{\dot{\beta}}} \sin\alpha \end{array}\right\} \text{Out-of-phase rolling derivatives}$$

$$\left.\begin{array}{l} C_{l_\beta} \sin\alpha - k^2 C_{l_{\dot{p}}} \\ C_{n_\beta} \sin\alpha - k^2 C_{n_{\dot{p}}} \\ C_{Y_\beta} \sin\alpha - k^2 C_{Y_{\dot{p}}} \end{array}\right\} \text{In-phase rolling derivatives}$$

$$\left.\begin{array}{l} C_{l_r} - C_{l_{\dot{\beta}}} \cos\alpha \\ C_{n_r} - C_{n_{\dot{\beta}}} \cos\alpha \\ C_{Y_r} - C_{Y_{\dot{\beta}}} \cos\alpha \end{array}\right\} \text{Out-of-phase yawing derivatives}$$

$$\left.\begin{aligned} &C_{l_\beta} \cos \alpha + k^2 C_{l_{\dot{r}}} \\ &C_{n_\beta} \cos \alpha + k^2 C_{n_{\dot{r}}} \\ &C_{Y_\beta} \cos \alpha + k^2 C_{Y_{\dot{r}}} \end{aligned}\right\} \text{In-phase yawing derivatives}$$

APPARATUS AND MODELS

The static and rotary oscillation tests were conducted in a low-speed tunnel which has a 12-foot octagonal cross section. Detailed descriptions of the oscillation apparatus and methods of obtaining and reducing the data are given in reference 3. The models were sting mounted and the forces and moments were measured about the body axes by three-component internal strain-gage balances. A sketch of the test setup for making the oscillation tests is shown in figure 2.

A three-view sketch of the model arrangement and a table of dimensions is presented in figure 3. The wings of the models were made of 0.125-inch aluminum alloy with 0.063R leading edges and the fuselages were made of 0.031-inch aluminum alloy. Because the purpose of this investigation was to determine the characteristics of the wings alone, the cross-sectional area of the fuselage-shaped fairing was kept to the minimum required to accommodate the balances. In addition to shielding the balances from the wind, the fairings provided longitudinal stiffness to the wings.

TESTS

All the static tests were made over an angle-of-attack range from -2.5° to 40° and the oscillation tests were made over an angle-of-attack range from 0° to 40°. No oscillation tests were made for the 70° swept wing. The static lateral characteristics were determined from runs made at various angles of attack over a sideslip range of $\pm 20^\circ$. The oscillation tests were made for a reduced frequency parameter k of 0.10 and rotary oscillation amplitudes of $\pm 5^\circ$.

The static tests were made at a dynamic pressure of 2.9 pounds per square foot which corresponds to an airspeed of 49.6 feet per second at standard sea-level conditions and to a test Reynolds number of 316,000 per foot. The oscillatory tests were run at a dynamic pressure of 3.4 pounds per square foot which corresponds to an airspeed of 53.6 feet per second and to a test Reynolds number of 342,000 per foot.

RESULTS AND DISCUSSION

Static Longitudinal Characteristics

The basic longitudinal characteristics of the wings are presented in figure 4. Cross plots of the variations of lift-curve slope with aspect ratio and of maximum value of L/D and of aerodynamic-center location with sweep angle are presented in figures 5, 6, and 7, respectively.

Lift and drag.- The data of figure 4 show that the lift-curve slope, the maximum lift-drag ratio and, in general, the maximum lift decreased with increasing sweep angle. A comparison between measured and theoretical variation in lift-curve slope at zero lift with aspect ratio is presented in figure 5. The measured values were taken from figure 4 and from references 1, 2, and 4 and the theoretical values were determined from the method of reference 5 which limits itself to aspect ratios below about 1.0, and from the method of reference 6 which is valid up to much higher aspect ratios. The measured values are in better agreement with the theory of reference 5 at the lower aspect ratios but approach the theory of reference 6 at the higher aspect ratios.

The variation of maximum lift-drag ratio with sweep angle is shown in figure 6. The data show a systematic decrease in the maximum value of L/D with increasing sweep angle.

Static longitudinal stability.- The data of figure 4 show that the static stability at low angles of attack increased slightly with sweep angle and that all the wings experienced a decrease in stability in the higher angle-of-attack range. The increase in stability with increasing sweep at low angles of attack is shown more clearly in figure 7 where the variation of aerodynamic center with sweep is plotted. The experimental values for the wings of this investigation are in good agreement with those of reference 1.

Static Lateral Characteristics

The variation of the coefficients C_Y, C_n, and C_l with angle of sideslip for various angles of attack is shown in figure 8. The curves are generally linear at the low angles of attack and become increasingly nonlinear with increase in angle of attack and increase in sweep. In addition to becoming nonlinear, the curves for the 82° and 84° sweep wings became asymmetrical about zero sideslip. This effect is attributed to asymmetrical disposition of vortices off the sharp nose which has been noted in other studies. (For example, see refs. 7 and 8.) The data of figure 8 are summarized in figure 9 in the form of the stability derivatives C_{Y_β}, C_{n_β}, and C_{l_β} plotted against angle of attack. In figure 10 the same derivatives are plotted against lift coefficient for the low lift coefficient range (0 to 0.6) where the derivatives are fairly linear for comparison with theory and other experimental data. The values of the derivatives were obtained by taking the difference between the values of the coefficients measured at sideslip angles of 5° and -5° except for the 82° and 84° swept wings.

In these cases an adjusted zero sideslip angle was assumed to make the curves symmetrical and the slopes were determined from coefficients measured at 5° and -5° from the adjusted zero, that is, in the steeper portions of the curves. Since some of the data are nonlinear, these derivatives should be used only to indicate trends and to provide approximate comparisons of the various wings.

Directional stability.- The data of figure 9 indicate that all of the wings have about the same low value of directional stability C_{n_β} up to an angle of attack of 15° or 20°, but increased sweep resulted in very high values of directional stability at high angles of attack for the wings swept 82° and 84°. The data presented in figure 10 show that there is a systematic increase in directional stability with sweep for the lift-coefficient range from about 0 to 0.6 except for the 84° wing. In this case, although the slope is greater than that of the 82° wing up to a lift coefficient of about 0.2, the directional stability decreases with further increase in C_L for the range shown. This is in qualitative agreement with the data of reference 1 which also show an increase in directional stability with sweep up to the most highly swept wing (82.9°) which also had an unstable break but at a lower lift coefficient. The variation found in the tests is in disagreement with the simple theory of reference 5 which gives a value of 0 for all conditions of sweep and lift coefficient.

Effective dihedral.- The data of figures 9 and 10 show that there is also a systematic increase in effective dihedral C_{l_β} with increasing sweep at lower angles of attack and that there were very large differences in the values of C_{l_β} for the various wings in the high angle-of-attack range. The variations of C_{l_β} with lift coefficient shown in figure 10 are essentially linear for the lift-coefficient range shown. The variation of C_{l_β}/C_L (the slopes from fig. 9) with aspect ratio from tests is compared with the theory of reference 5 in figure 11. The test results show the same trend as the theory but the experimental values are approximately one-third lower than the calculated values.

Side force.- The data of figures 9 and 10 show that all the wings had about the same small negative value of side-force parameter C_{Y_β} at low angles of attack. As the angle of attack increased C_{Y_β} became positive for all the wings, the values being greater for the more highly swept wings.

Oscillatory Lateral Stability Derivatives

Out-of-phase derivatives.- The variation of the out-of-phase rolling and yawing oscillation derivatives with angle of attack is presented in figure 12. A cross plot of these data (fig. 13) shows the variation of the derivatives with aspect ratio for various lift coefficients. Also shown on the figure are the theoretical values of these derivatives for one lift coefficient as determined from the method of reference 5. These data show that at the higher aspect ratios (lowest sweep angles) the values of the derivatives were generally small and relatively unaffected by lift coefficient. As the aspect ratio was reduced, however, increases in lift coefficient resulted in very large changes in the

derivatives. The theoretical prediction of the derivatives appears to be fairly good except in the case of $C_{l_r} - C_{l_{\dot{\beta}}} \cos \alpha$ where tests show a variation from positive values to negative values with increasing sweep, whereas the theory shows increasing positive values with increasing sweep. The difference between theory and tests at large sweep angles becomes more pronounced with increase in lift coefficient. The trend of the experimental data shown in figure 13 for this derivative is in qualitative agreement with the experimental data of reference 7.

In-phase derivatives.- The variation of the in-phase rolling and yawing derivatives with angle of attack is presented in figure 14. The corresponding parameters obtained from static tests are compared with the oscillation derivatives for one representative case, the 80° swept wing, in figure 15. The data show good agreement except at the higher angles of attack where the differences in static and oscillatory data may be attributed to flow separation.

SUMMARY OF RESULTS

The results of a low subsonic investigation of the stability characteristics of a series of thin flat-plate delta wings having leading-edge sweep angles from 70° to 84° can be summarized as follows:

1. The static longitudinal stability, the directional stability, and effective dihedral increased with increasing sweep angle. The static lateral derivatives were linear at low angles of attack and became increasingly nonlinear with increase in angle of attack and increase in sweep. The longitudinal stability and effective dihedral generally increased as predicted by theory.

2. The values of the rolling and yawing oscillation derivatives were generally small and relatively unaffected by change in lift coefficient for the lowest sweep angles. As sweep was increased, increases in lift coefficient resulted in very large changes in the values of the out-of-phase derivatives. The theoretical prediction of the derivatives at low lift coefficients appears to be fairly good except for the case of C_{l_r} at the higher sweep angles where the experimental and theoretical results showed opposite trends.

Langley Research Center,
National Aeronautics and Space Administration,
Langley Station, Hampton, Va., April 25, 1963.

REFERENCES

1. Tosti, Louis P.: Low-Speed Static Stability and Damping-in-Roll Characteristics of Some Swept and Unswept Low-Aspect-Ratio Wings. NACA TN 1468, 1947.

2. Letko, William: Experimental Determination at Subsonic Speeds of the Oscillatory and Static Lateral Stability Derivatives of a Series of Delta Wings With Leading-Edge Sweep From 30° to 86.5°. NACA RM L57A30, 1957.

3. Hewes, Donald E.: Low-Subsonic Measurements of the Static and Oscillatory Lateral Stability Derivatives of a Sweptback-Wing Airplane Configuration at Angles of Attack From -10° to 90°. NASA MEMO 5-20-59L, 1959.

4. Peckham, D. H.: Low-Speed Wind-Tunnel Tests on a Series of Uncambered Slender Pointed Wings With Sharp Edges. R. & M. No. 3186, British A.R.C., 1961.

5. Ribner, Herbert S.: The Stability Derivatives of Low-Aspect-Ratio Triangular Wings at Subsonic and Supersonic Speeds. NACA TN 1423, 1947.

6. Lowry, John G., and Polhamus, Edward C.: A Method for Predicting Lift Increments Due to Flap Deflection at Low Angles of Attack in Incompressible Flow. NACA TN 3911, 1957.

7. Letko, William: A Low-Speed Experimental Study of the Directional Characteristics of a Sharp-Nosed Fuselage Through a Large Angle-of-Attack Range at Zero Angle of Sideslip. NACA TN 2911, 1953.

8. Boisseau, Peter C.: Investigation of the Low-Subsonic Flight Characteristics of a Model of a Supersonic Airplane Configuration Having Tail Surfaces Outboard of the Wing Tips. NASA TM X-541, 1961.

10

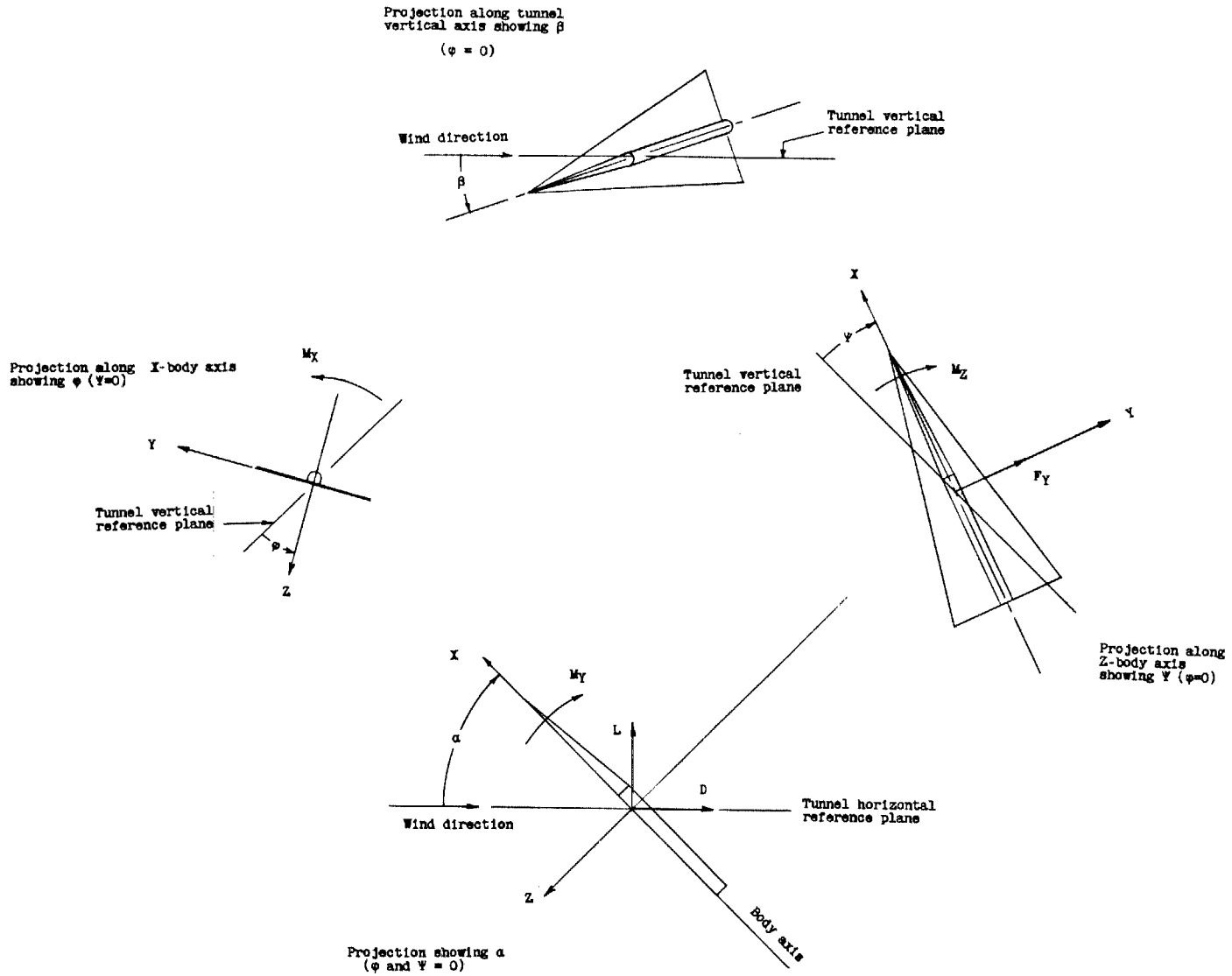

Figure 1.- The body system of axes. Arrows indicate positive directions of moments, forces, and angles. This system of axes is defined as an orthogonal system having the origin at the center of gravity and in which the X-axis is in the plane of symmetry and alined with the longitudinal axis of the fuselage, the Z-axis is in the plane of symmetry and perpendicular to the X-axis, and the Y-axis is perpendicular to the plane of symmetry.

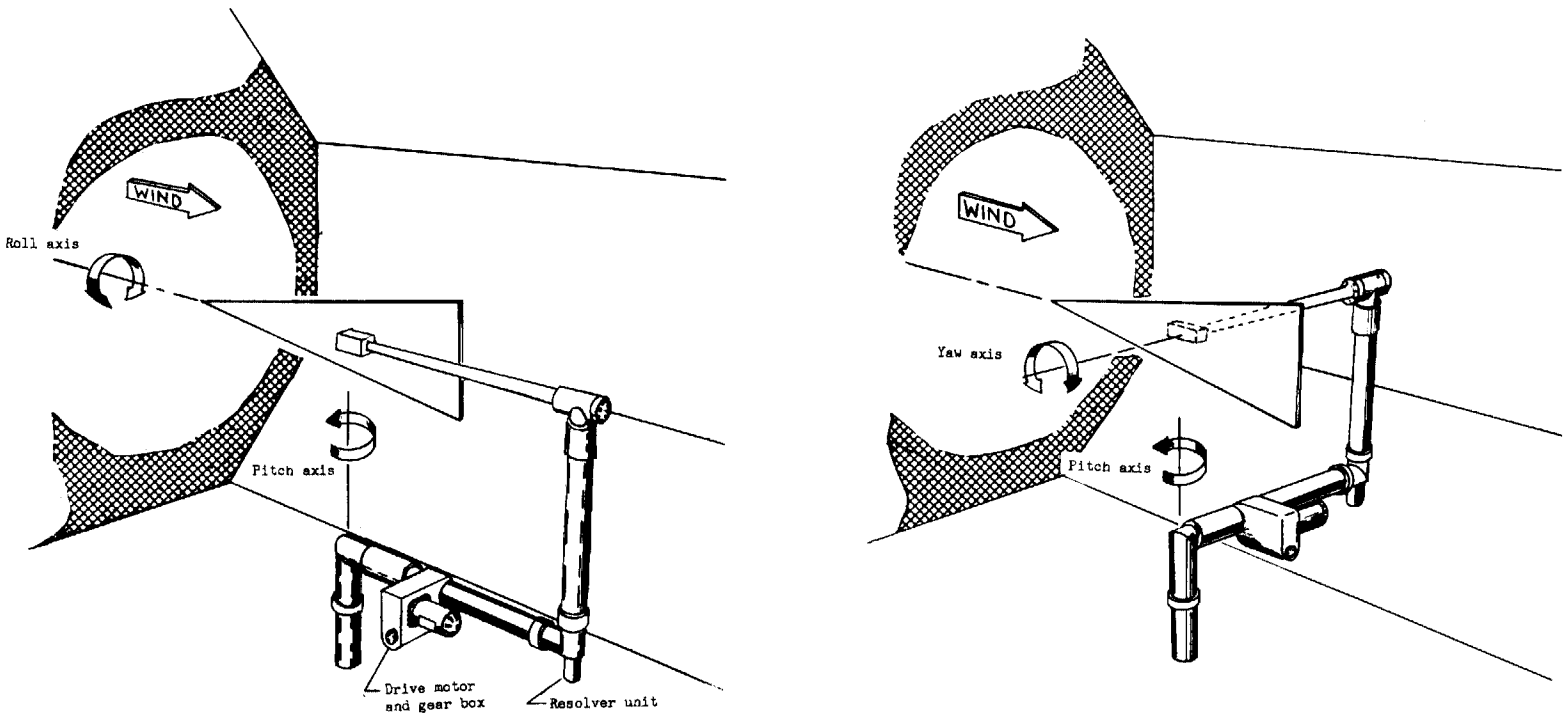

(a) Arrangement for rotary oscillation tests in roll.

(b) Arrangement for rotary oscillation tests in yaw.

Figure 2.- Schematic sketch of the oscillation test apparatus.

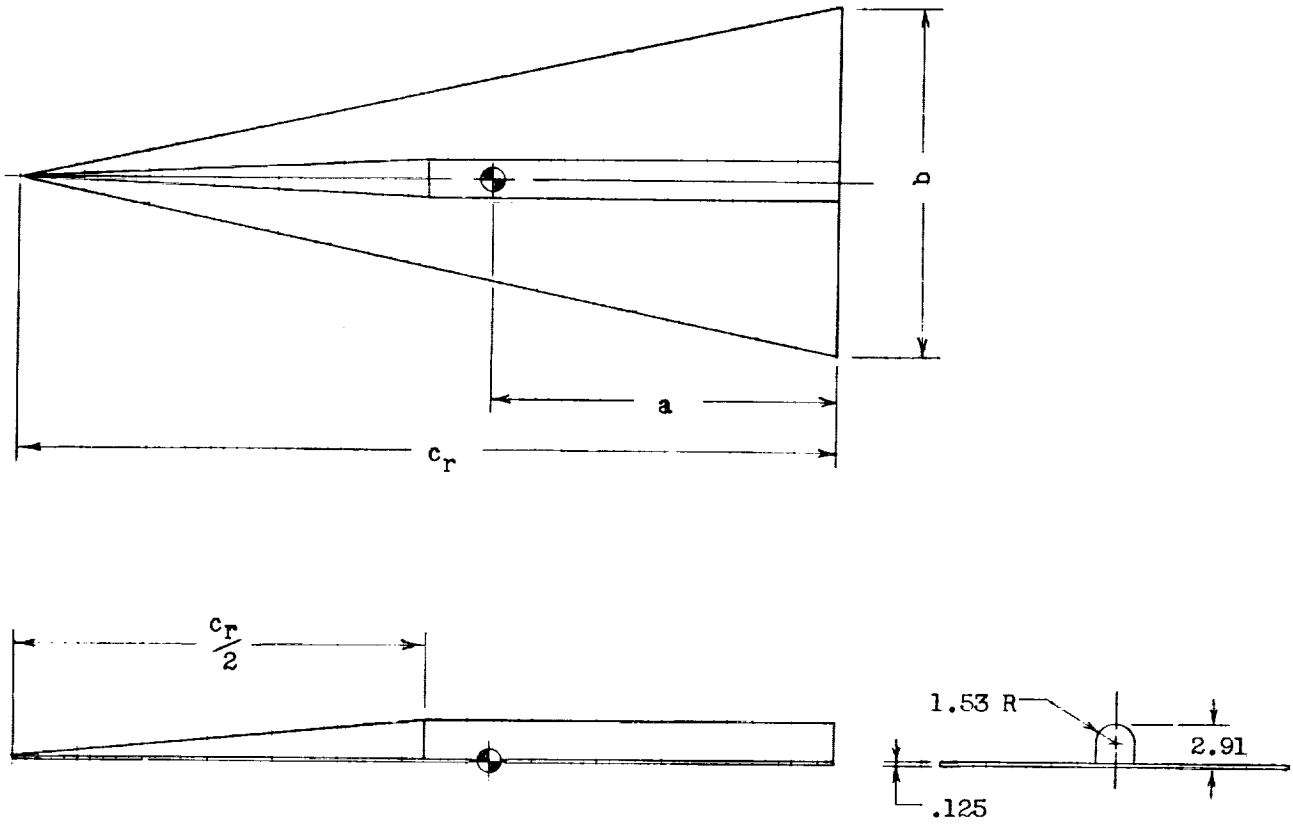

Leading-edge sweep, Λ, deg	Aspect ratio	Span, b, in	Root chord, c_r, in.	$\bar{c}$, in.	Wing area, sq. in.	a, in.
70	1.46	35.20	48.36	32.24	851.3	19.30
76	1.00	29.14	58.44	38.98	"	23.39
78	0.85	26.91	63.28	42.21	"	25.32
80	0.71	24.70	69.49	46.35	"	27.81
82	0.56	21.87	77.84	51.92	"	31.15
84	0.42	18.92	90.00	60.00	"	36.00

Figure 3.- Sketch showing details of the models used in the tests.

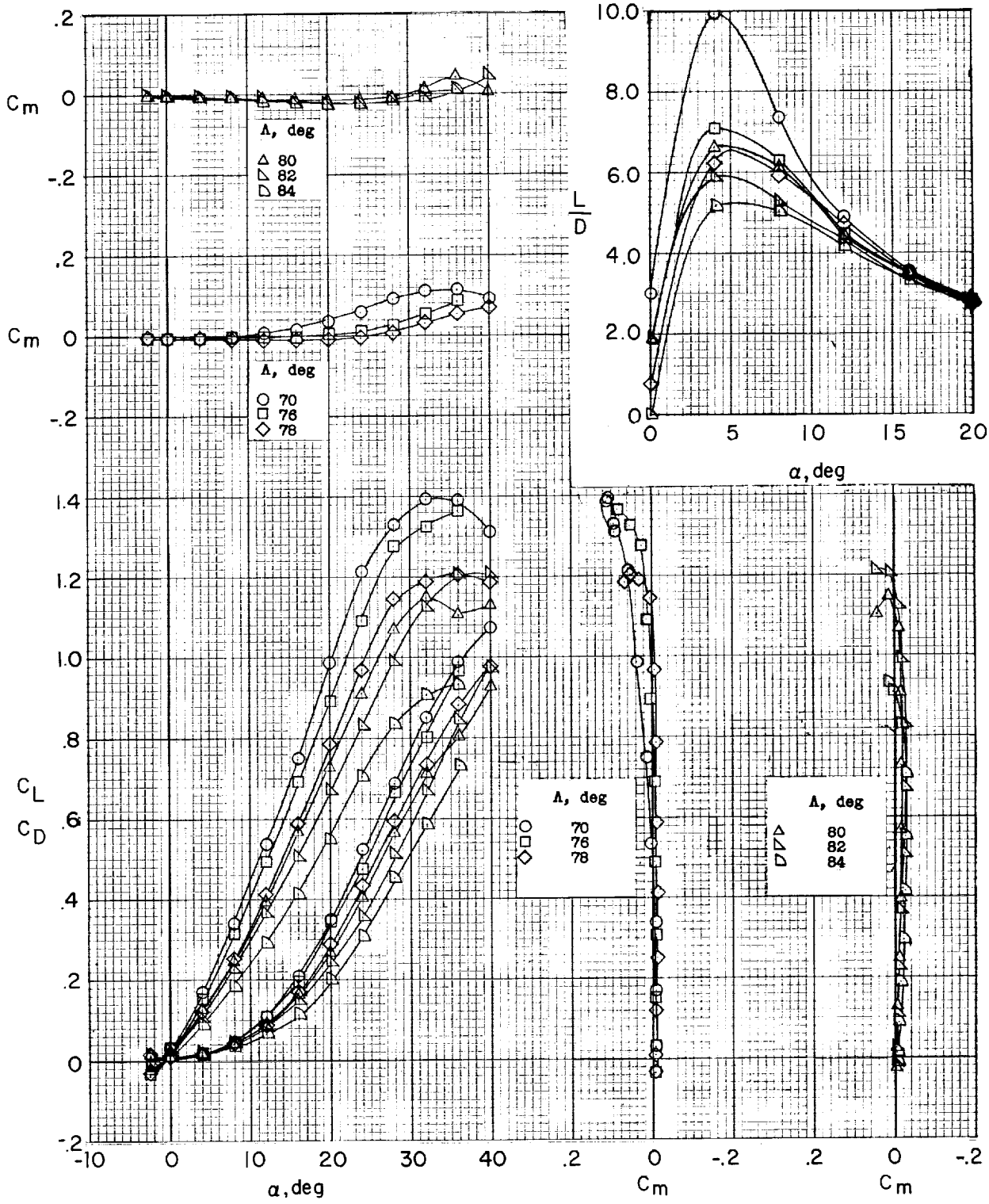

Figure 4.- Effect of sweep angle on the static longitudinal characteristics of the wings tested.

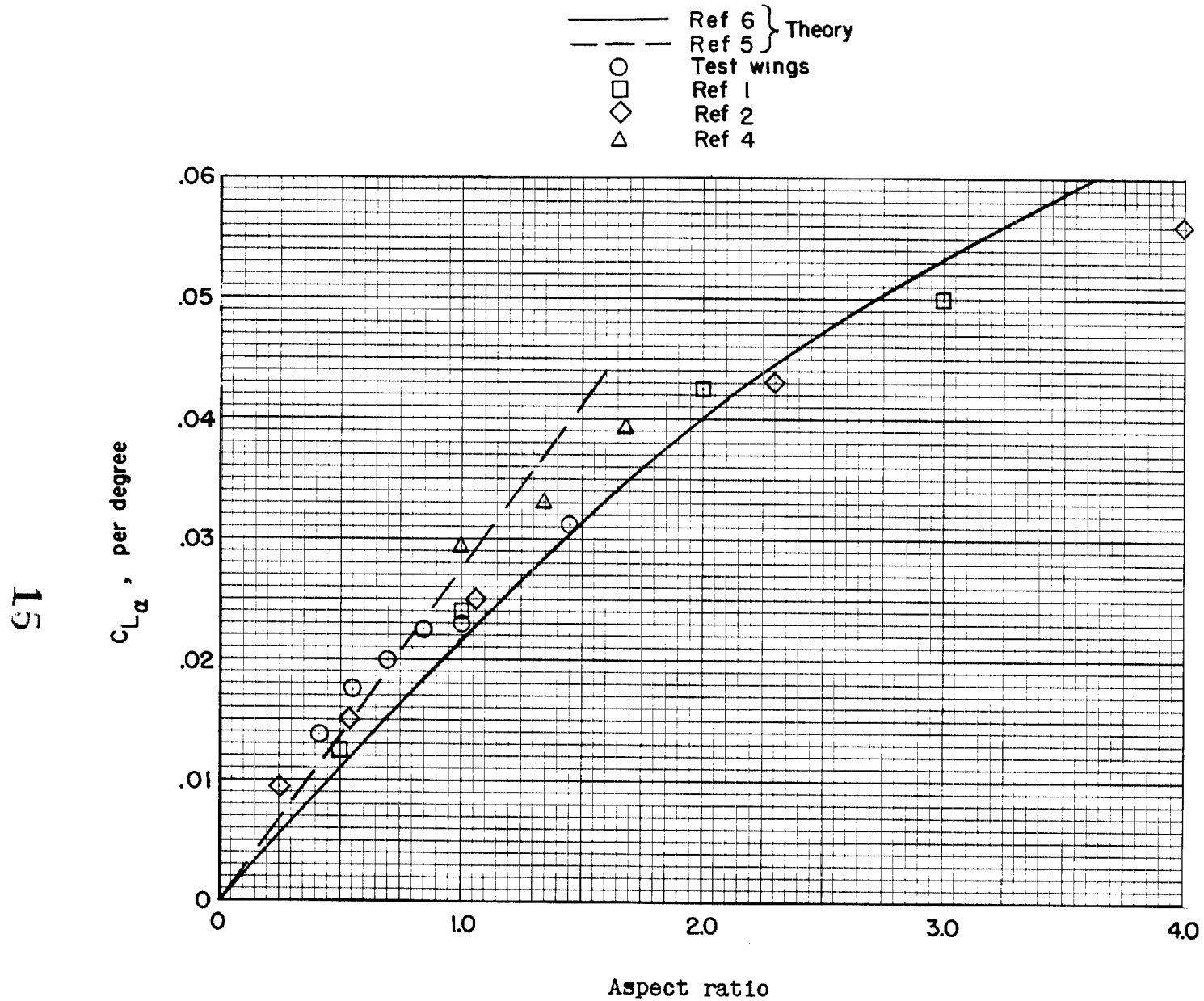

Figure 5.- Variation of lift-curve slope with aspect ratio at $C_L = 0$.

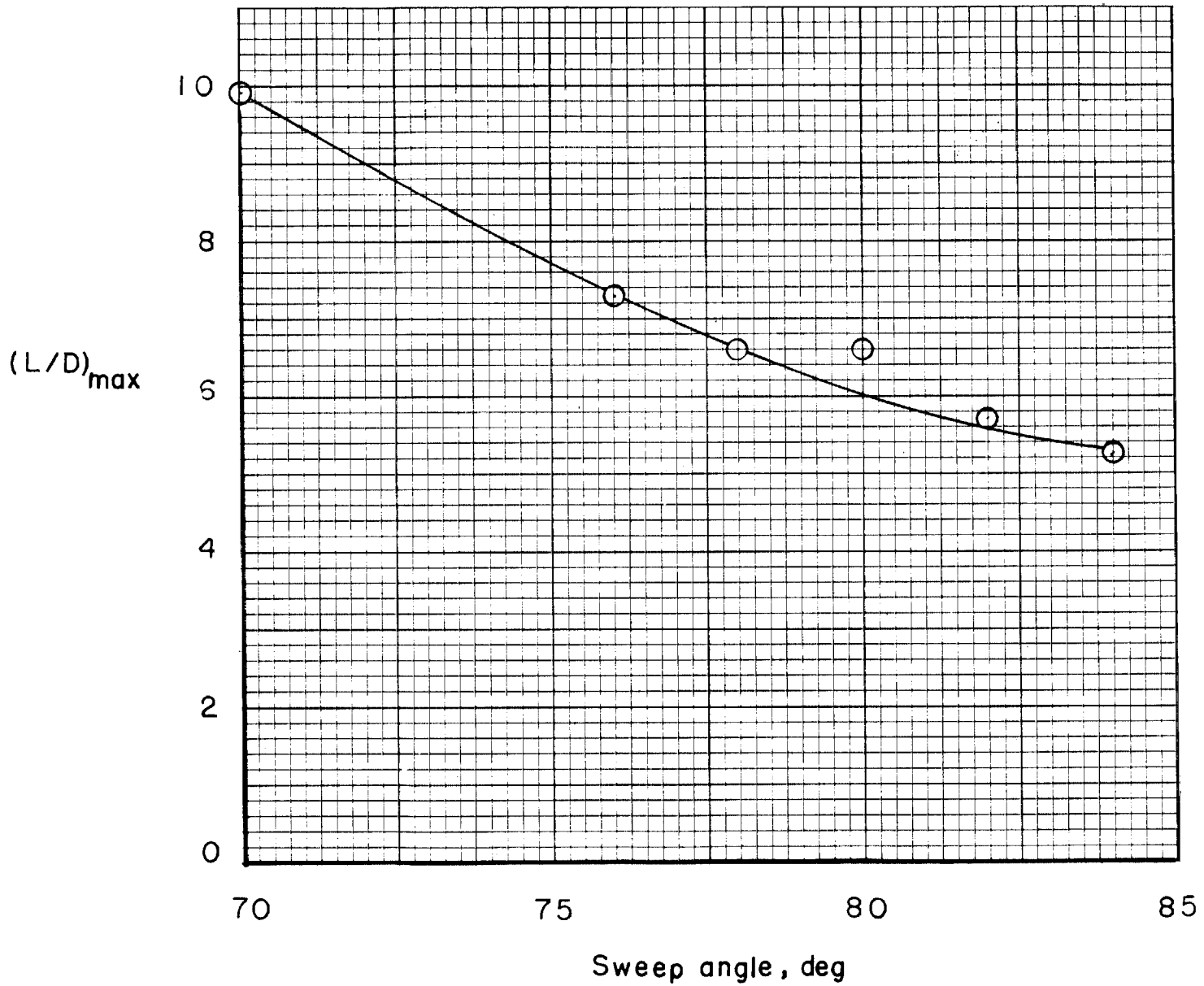

Figure 6.- Variation of maximum L/D value with leading-edge sweep angle.

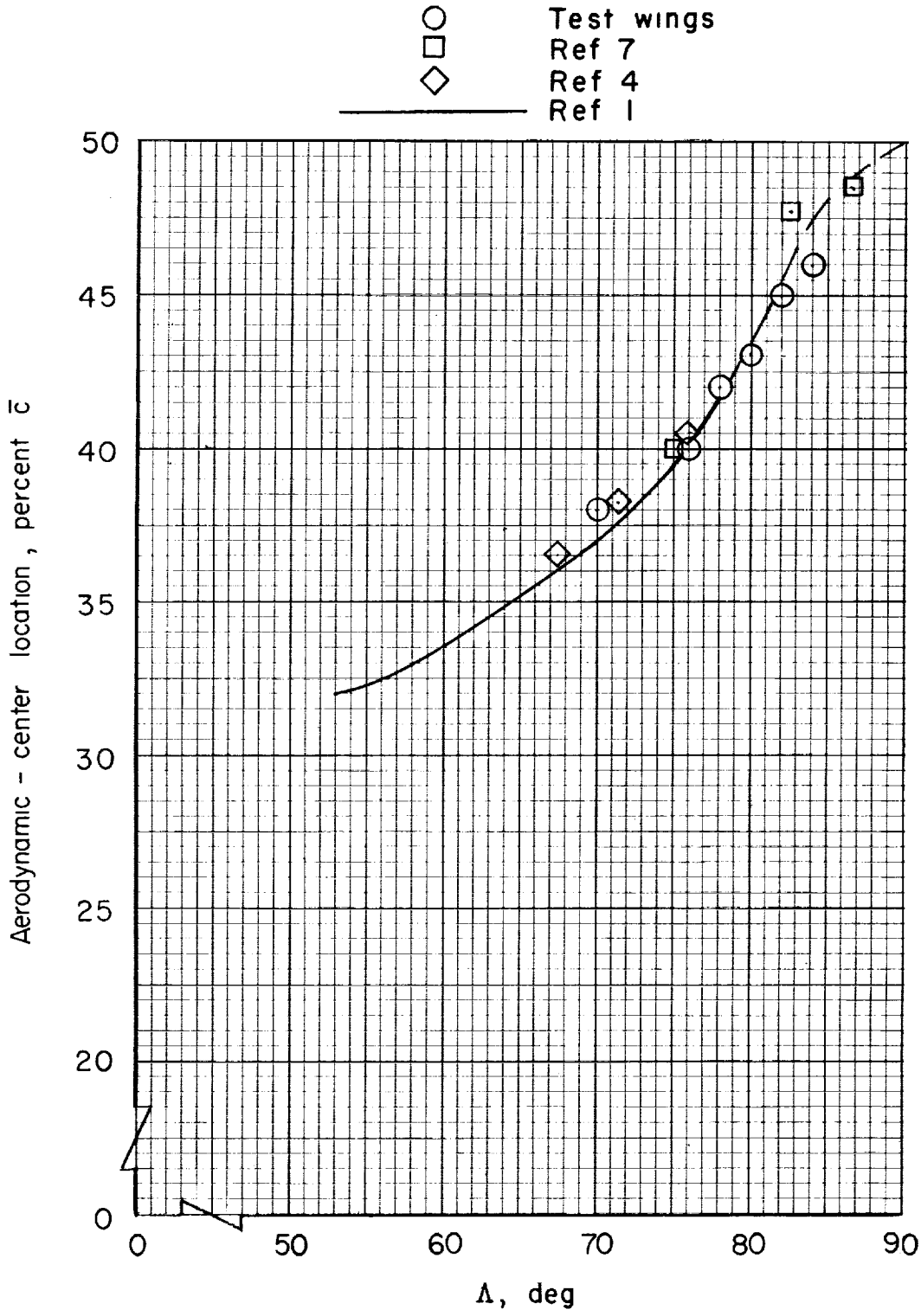

Figure 7.- Variation of aerodynamic-center location with leading-edge sweep. $\alpha = 0^{\circ}$ to 8°.

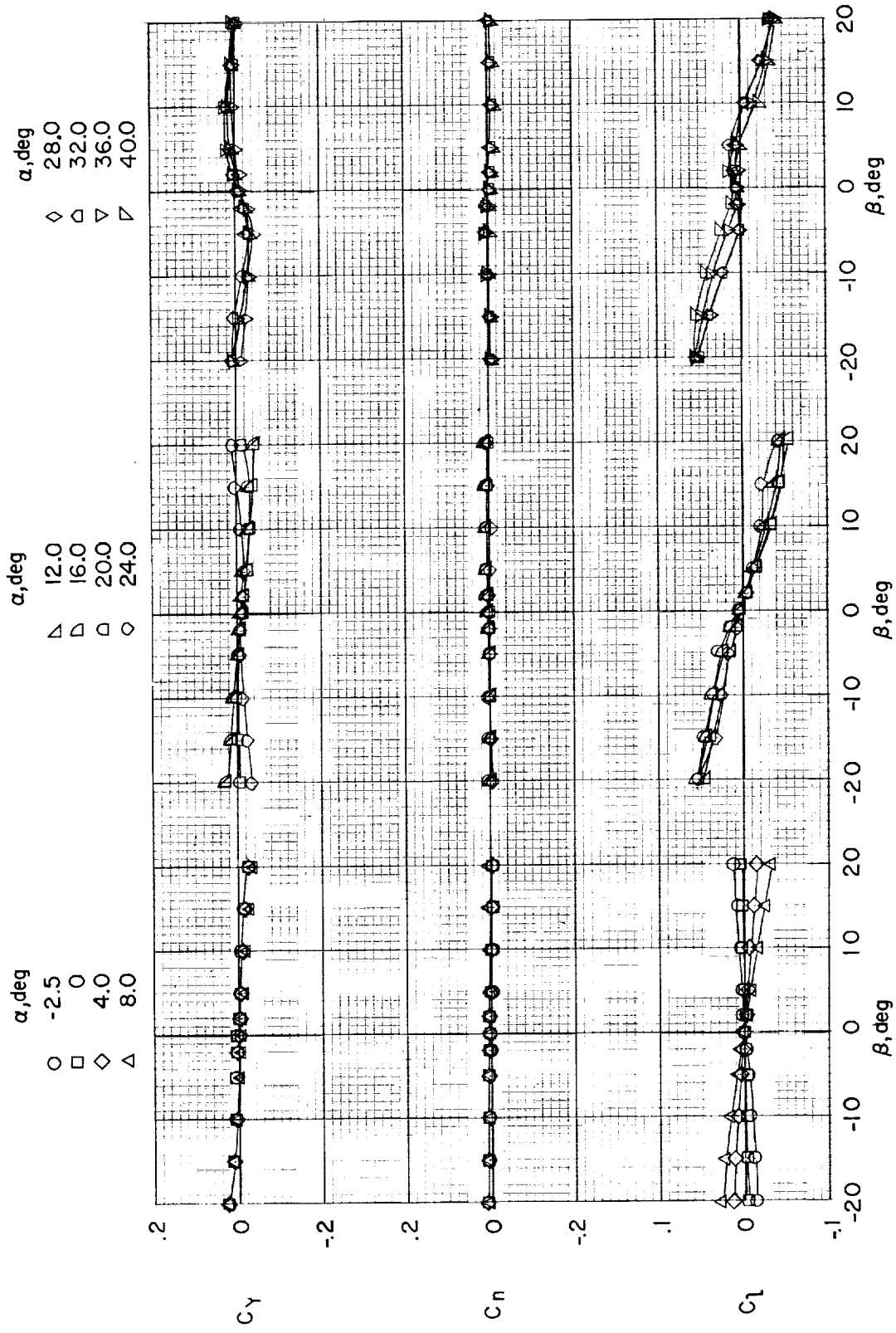

(a) $\Lambda = 70^{\circ}$.

Figure 8.- Variation of lateral coefficients of the wings with angle of sideslip.

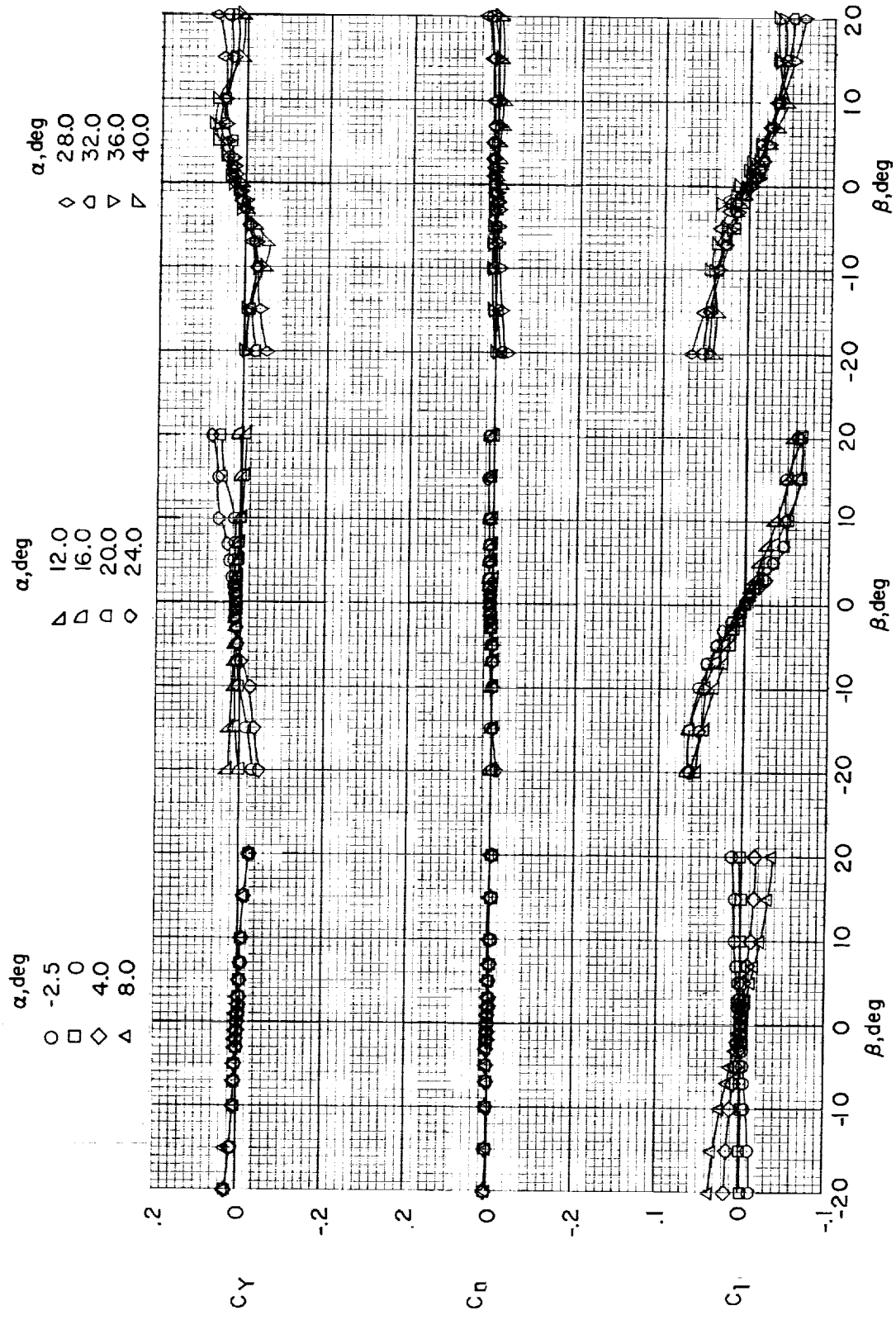

(b) $\Lambda = 76^{\circ}$.

Figure 8.- Continued.

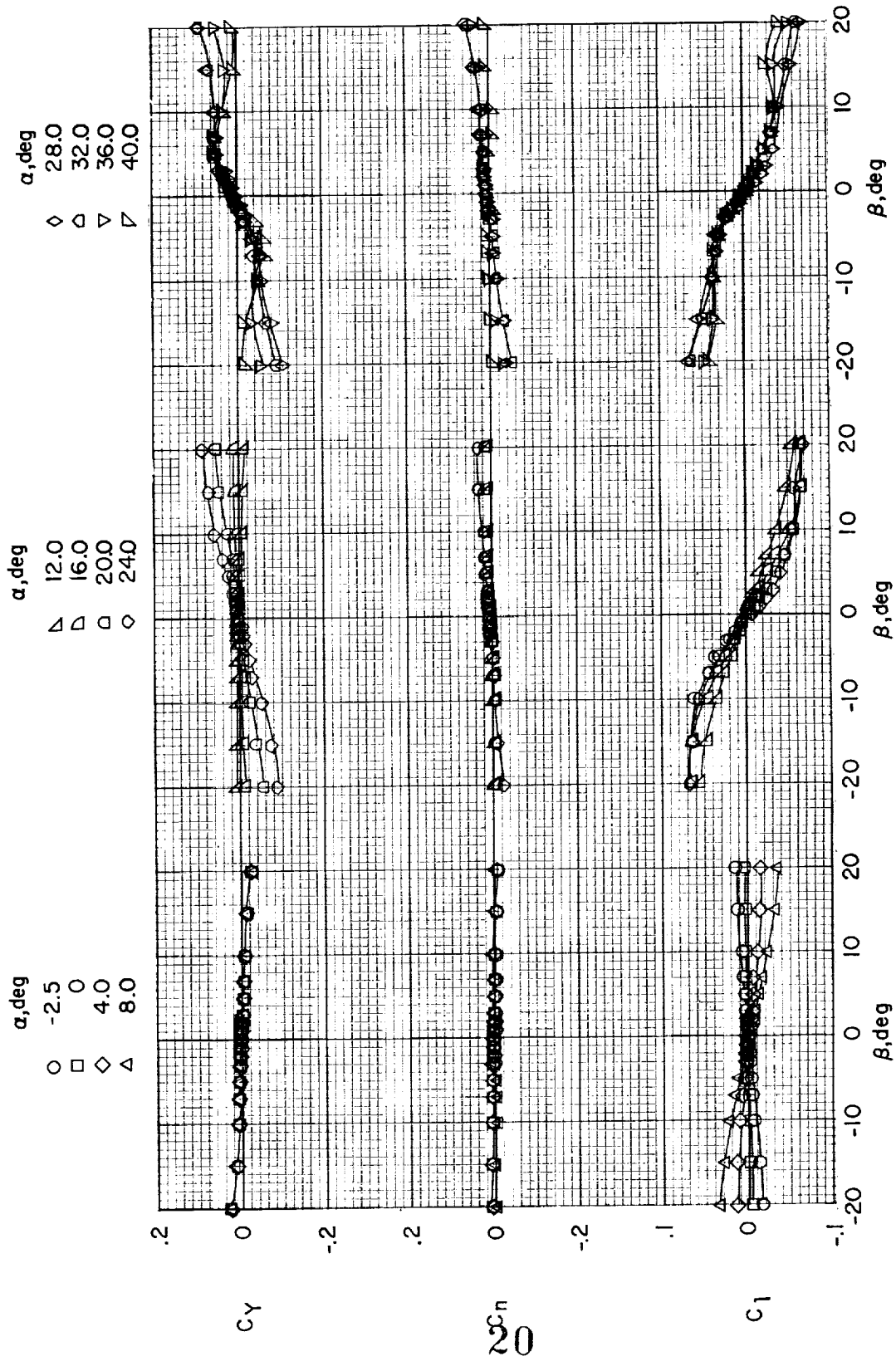

(c) $\Lambda = 78^\circ$.

Figure 8.- Continued.

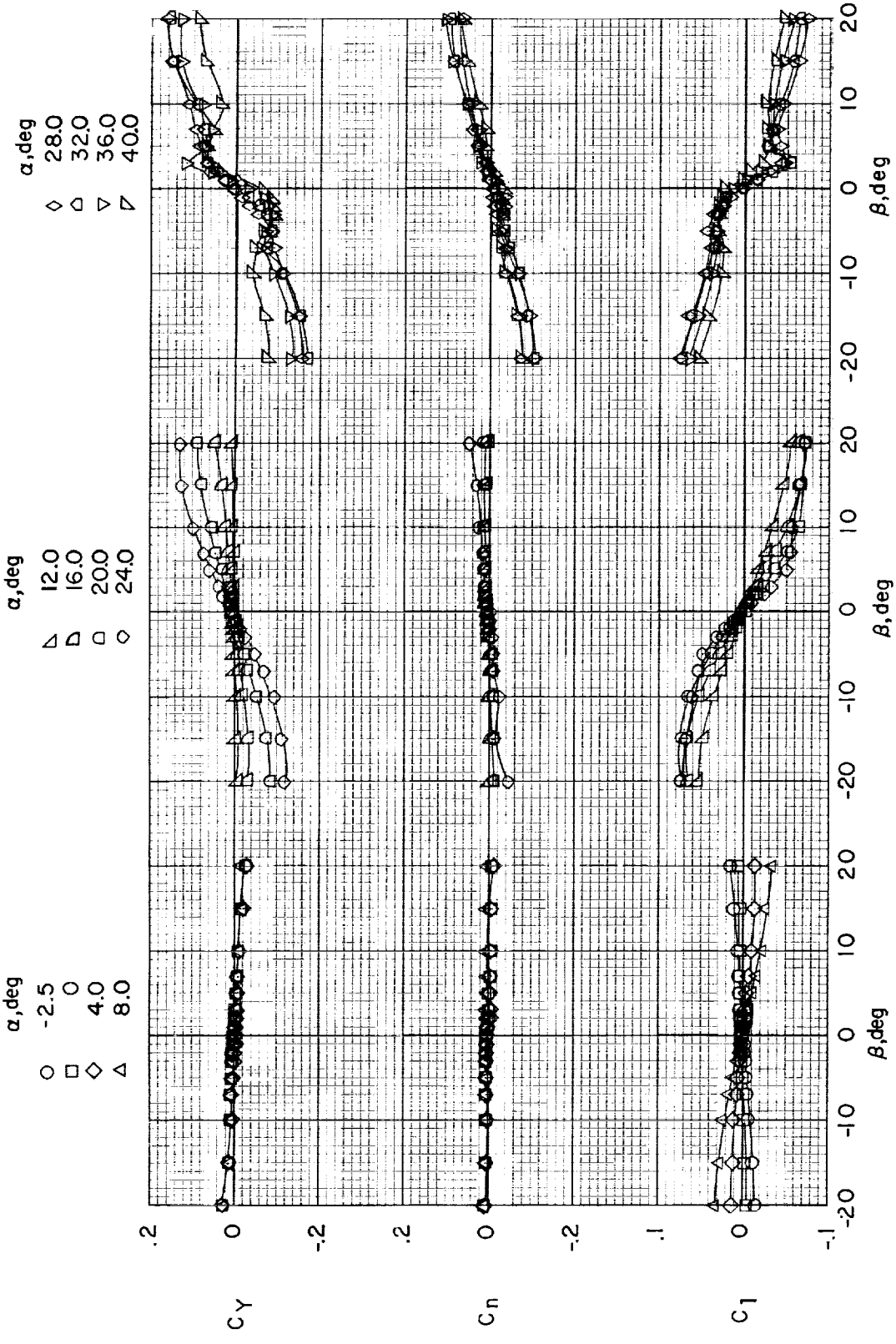

(d) $\Lambda = 80^{\circ}$.

Figure 8.- Continued.

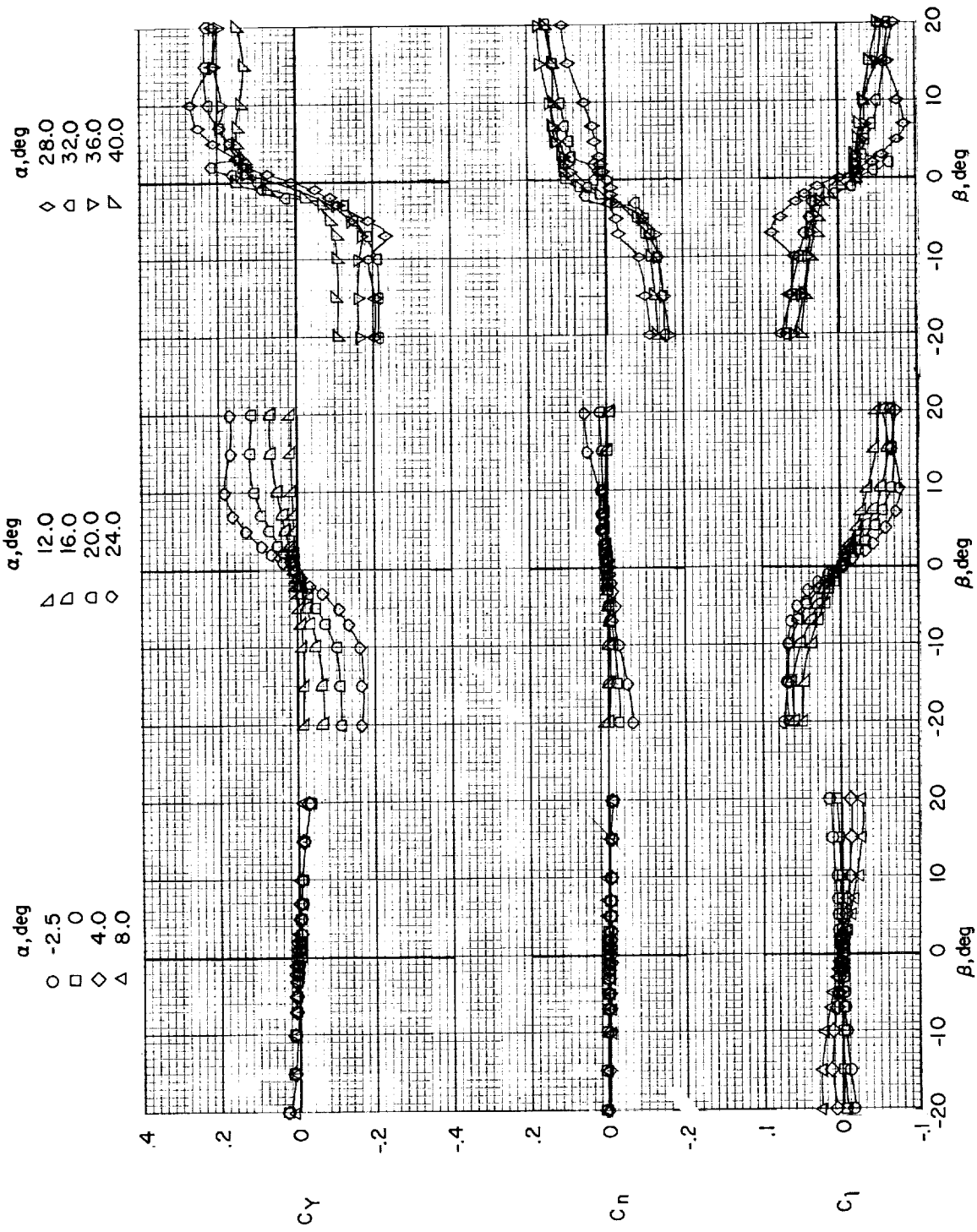

(e) $\Lambda = 82°$.

Figure 8.- Continued.

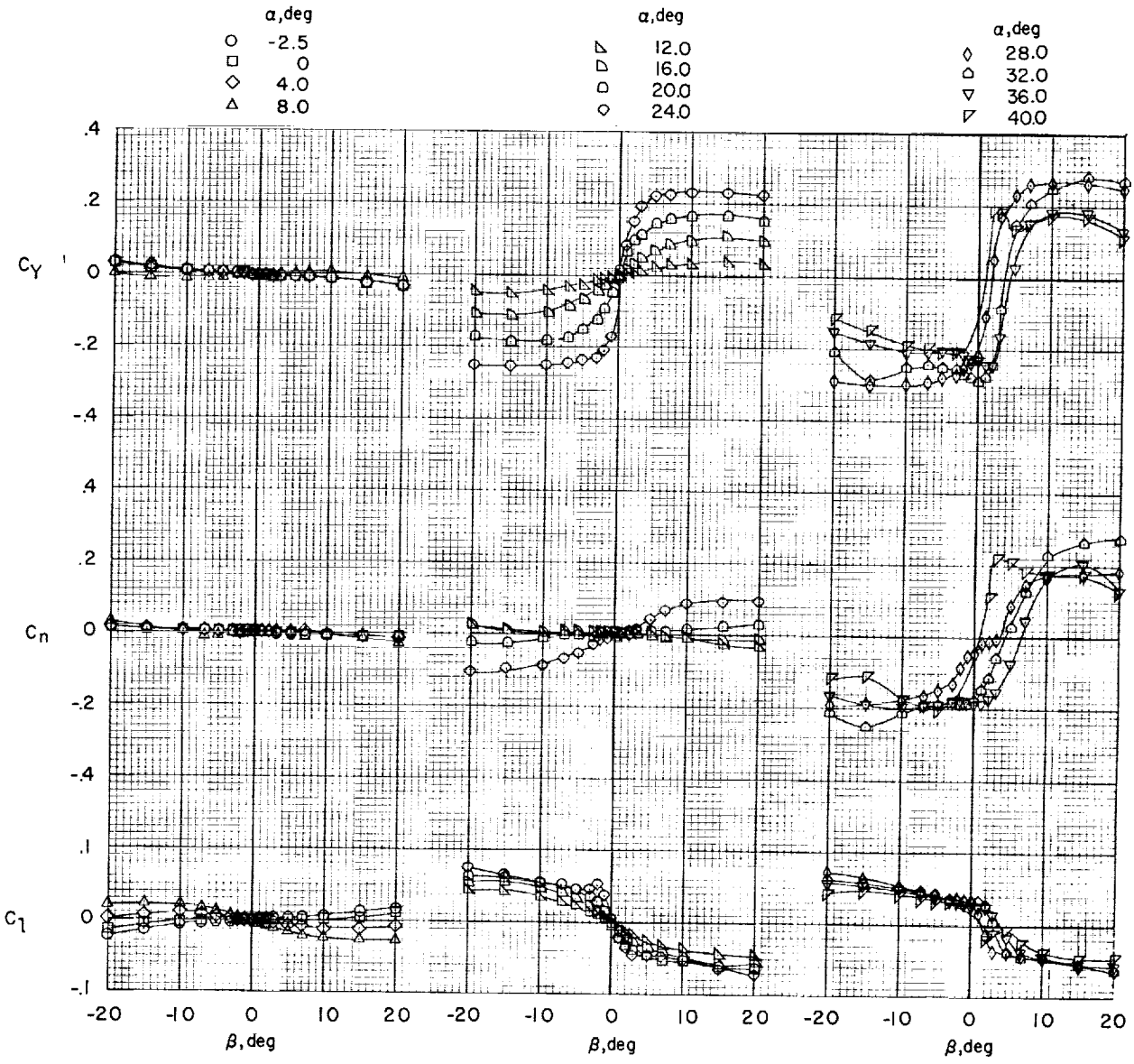

(f) $\Lambda = 84^\circ$.

Figure 8.- Concluded.

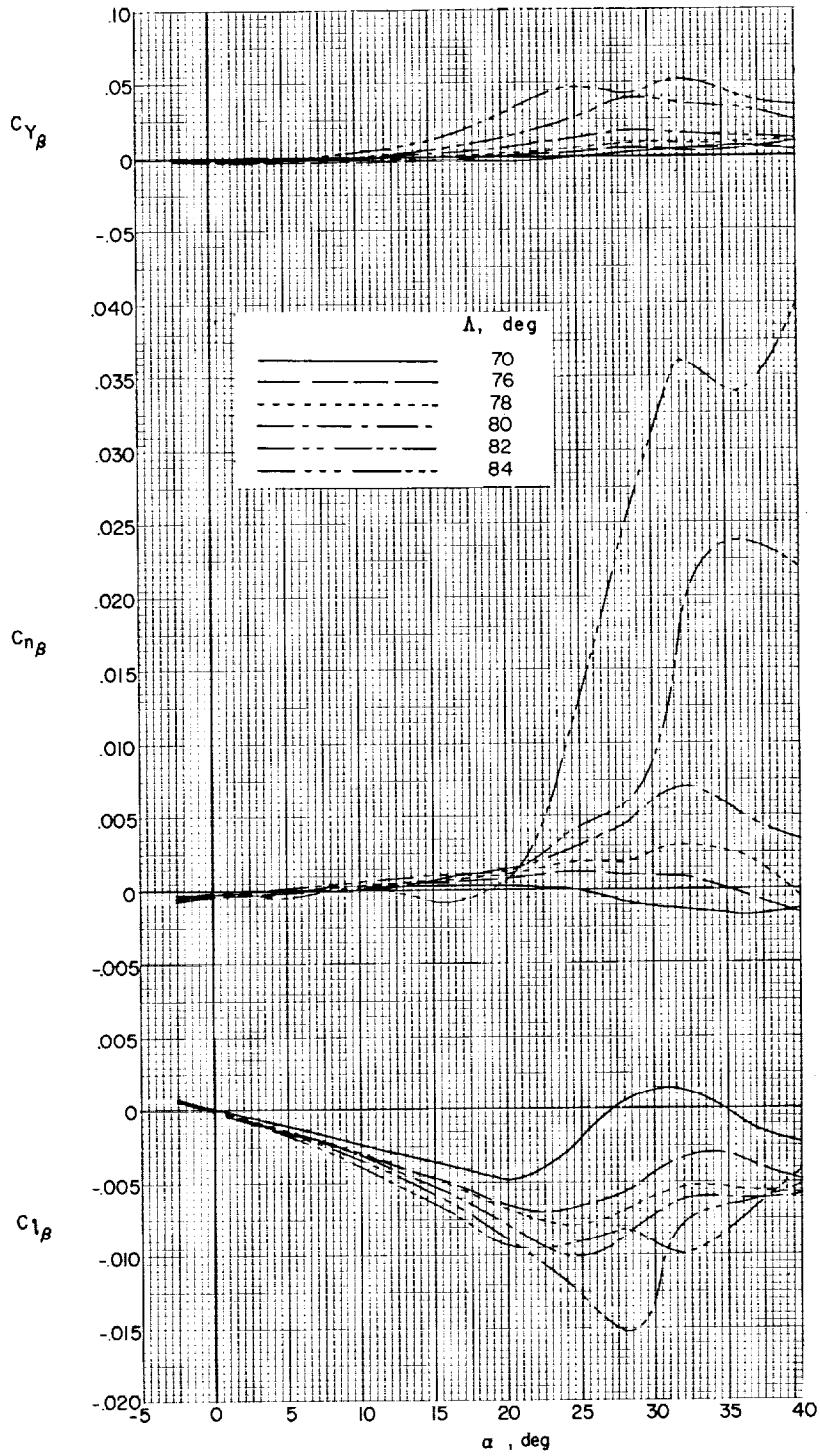

Figure 9.- Variation of experimental static lateral stability derivatives with angle of attack. $\beta = \pm 5^\circ$; plotted per degree.

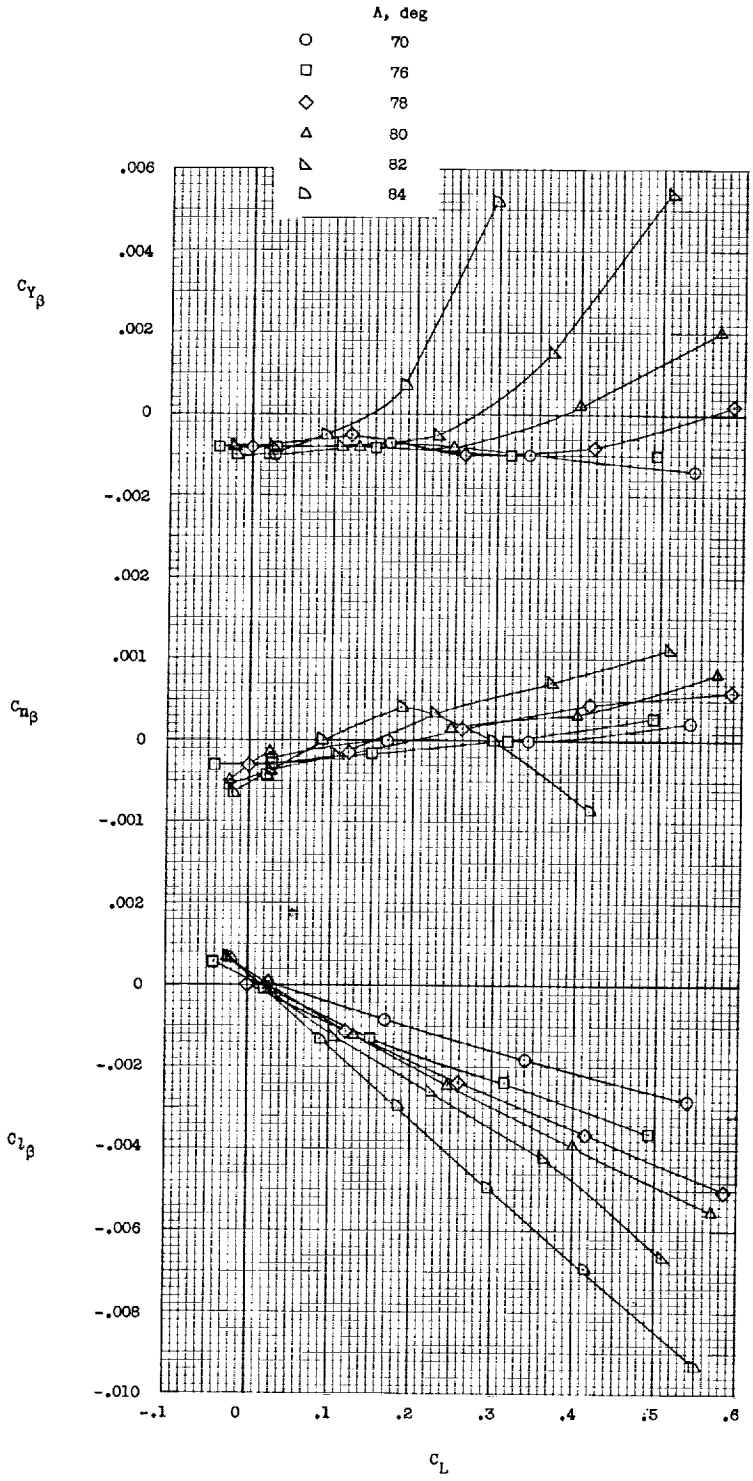

Figure 10.- Variation of static lateral stability derivatives with lift coefficient. $\beta = \pm 5^\circ$; plotted per degree.

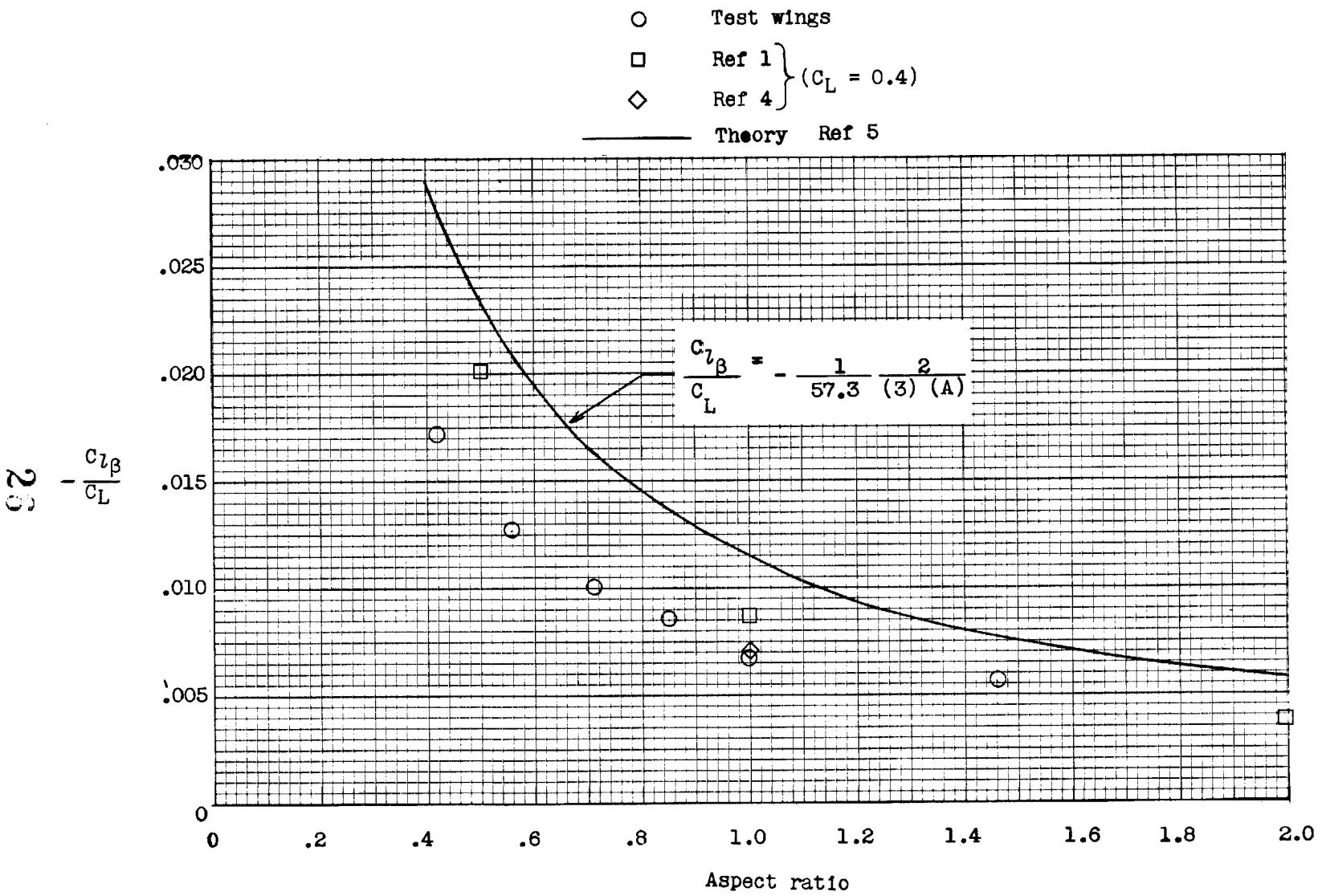

Figure 11.- Variation of effective dihedral parameter with aspect ratio at angles of attack between 0° and 16°. C_L = 0 to 0.4.

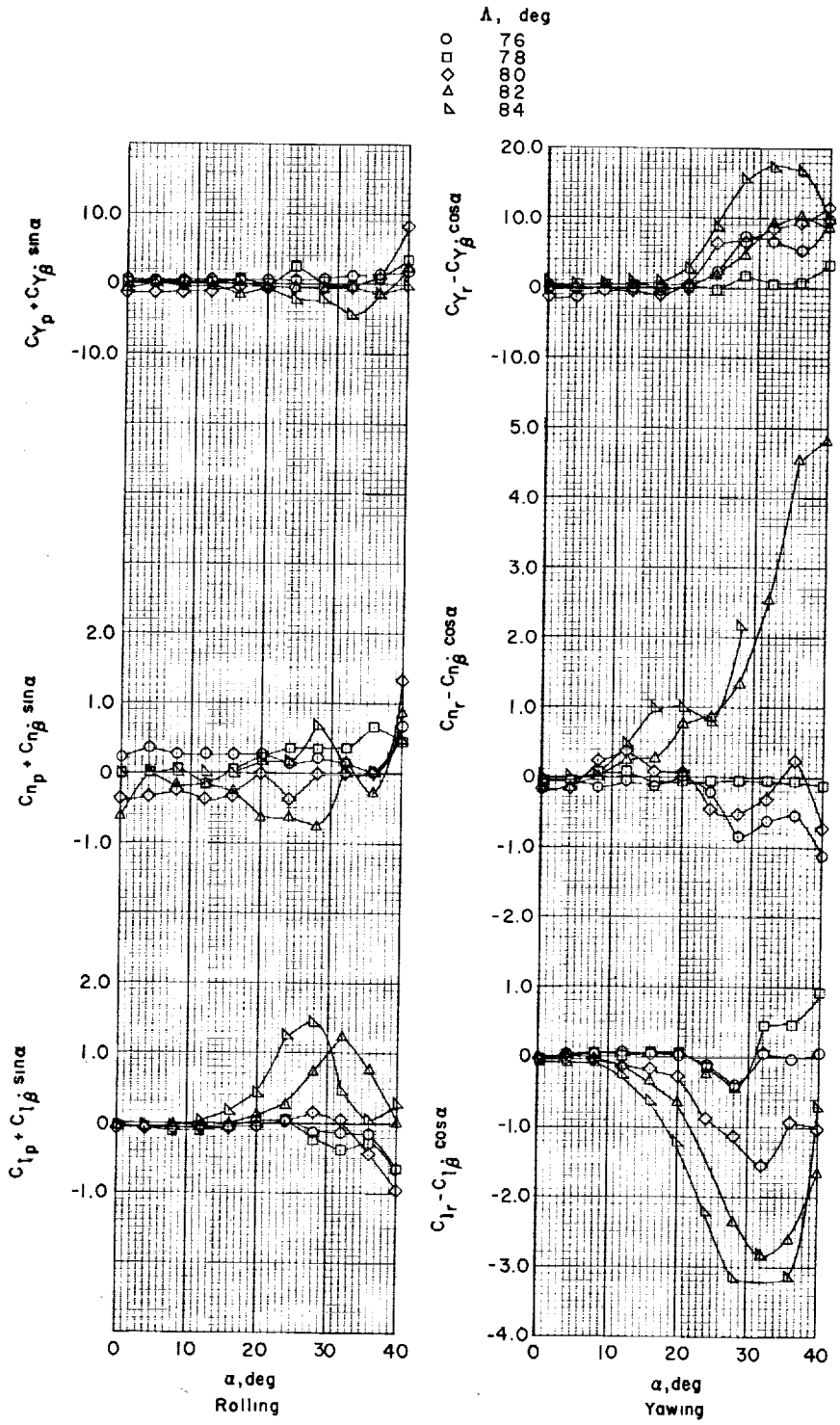

Figure 12.- Variation of out-of-phase rolling and yawing oscillation derivatives with angle of attack. Plotted per radian.

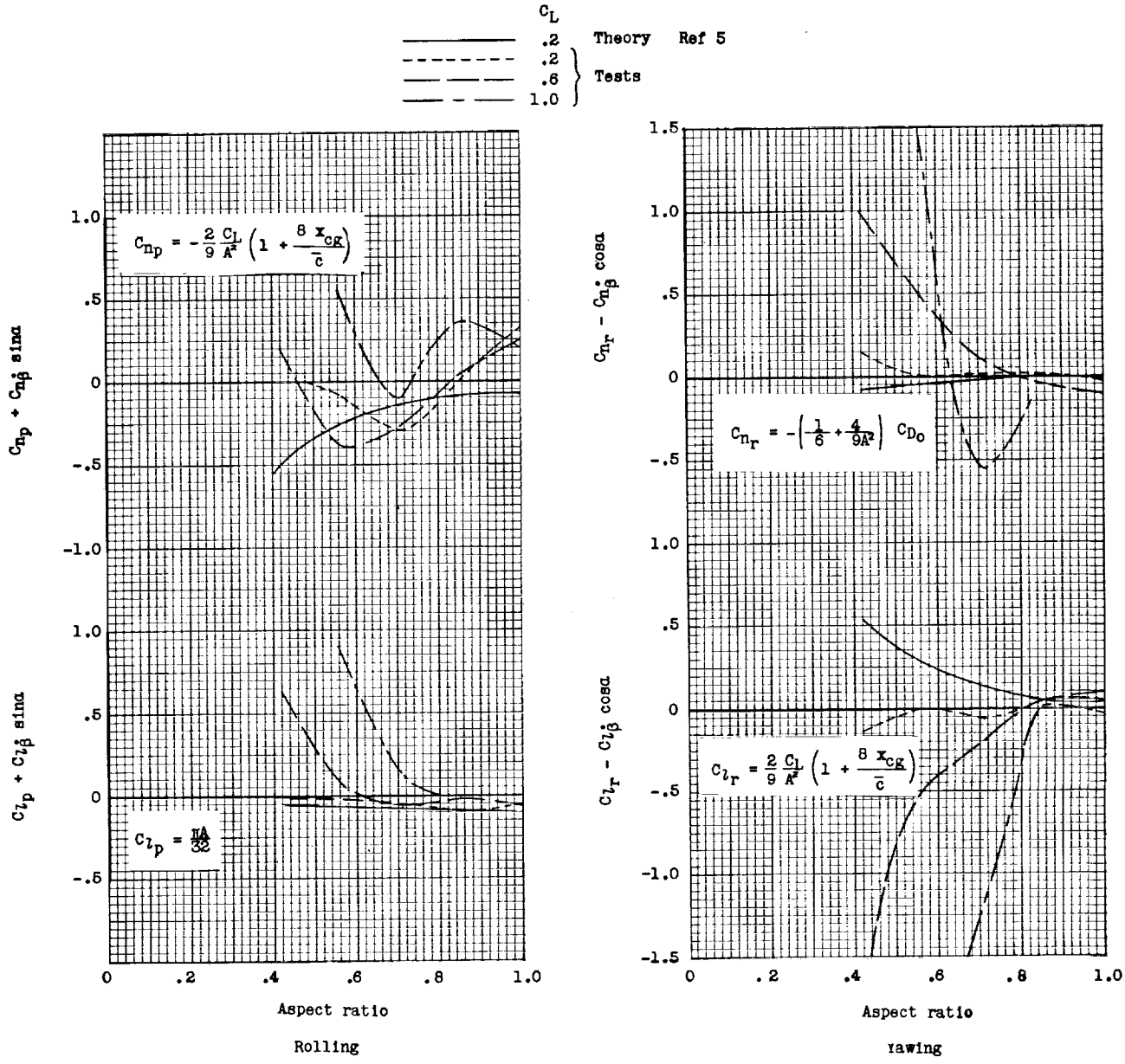

Figure 13.- Variation of rolling and yawing oscillation derivatives with aspect ratio.

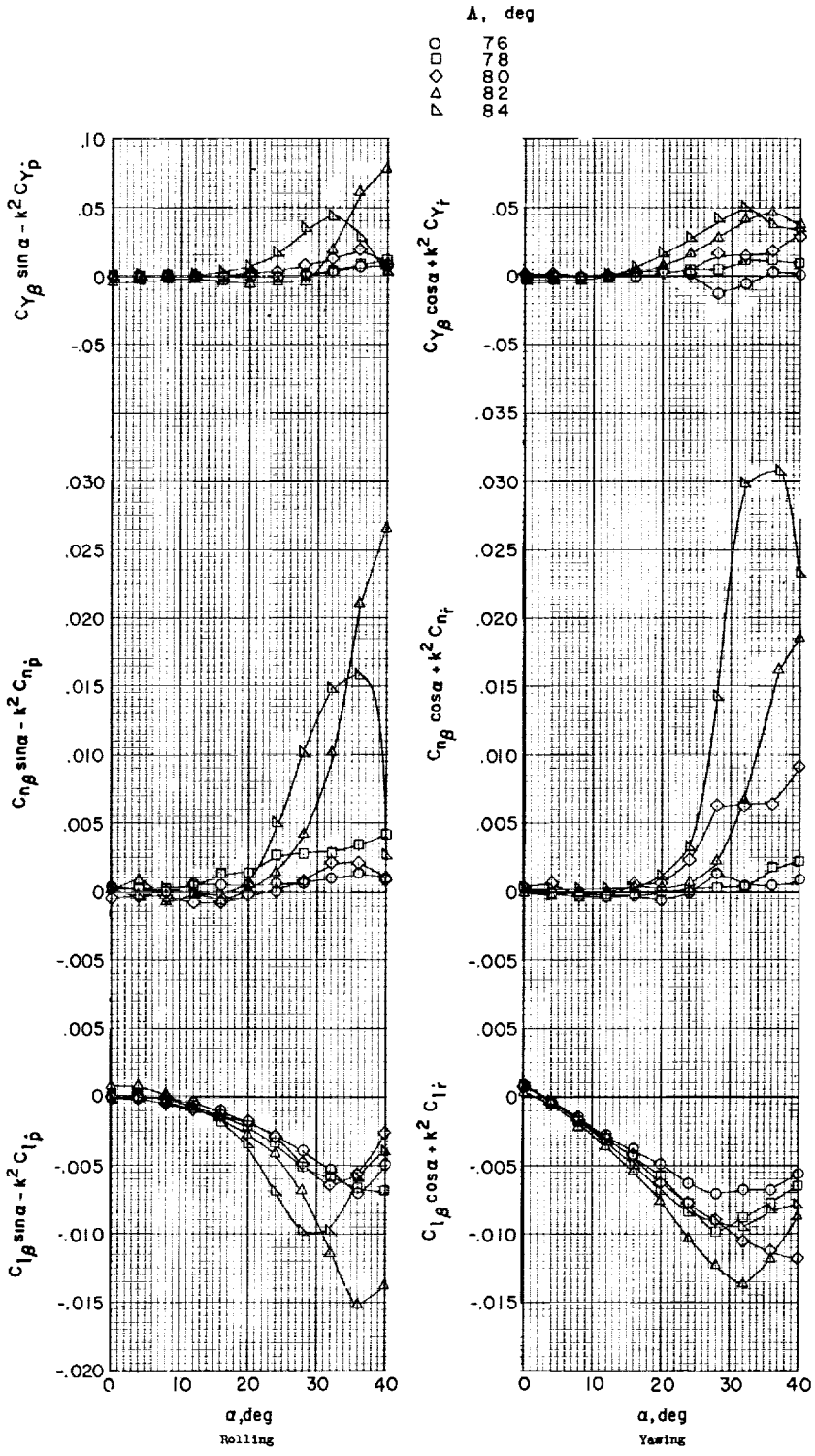

Figure 14.- Variation of in-phase rolling and yawing oscillation derivatives with angle of attack. Plotted per degree.

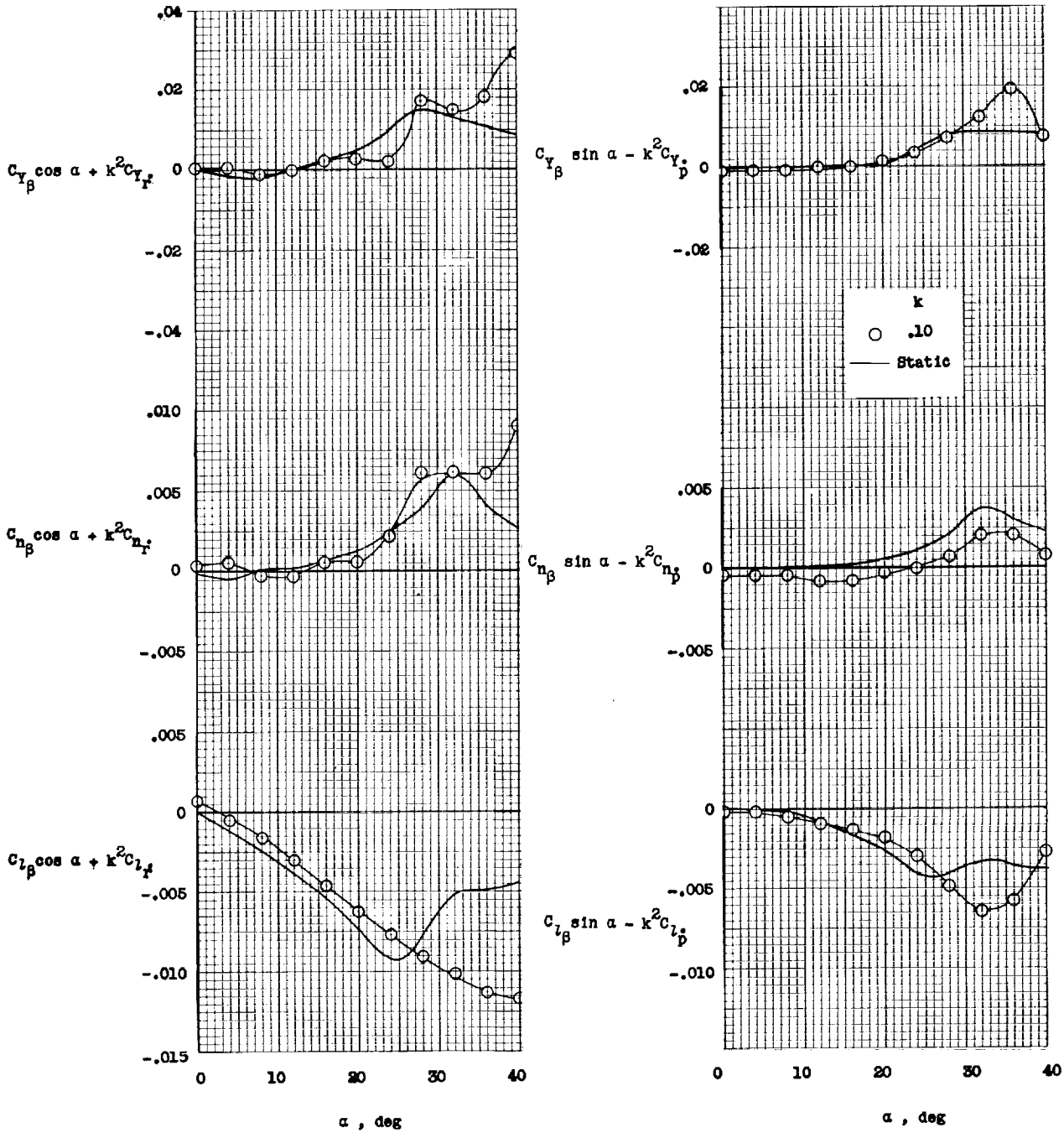

(a) Yawing.

(b) Rolling.

Figure 15.- Comparison of the in-phase rolling and yawing derivatives with static-force test data for the 80° swept wing.

NASA-Langley, 1963 L-3008